Intensive Care Med (2000) 26: 857–869

ORIGINAL

L. Puybasset
P. Cluzel
P. Gusman
P. Grenier
F. Preteux
J.-J. Rouby
and the CT Scan ARDS Study Group

Regional distribution of gas and tissue in acute respiratory distress syndrome. I. Consequences for lung morphology

Received: 12 May 1999
Final revision received: 9 February 2000
Accepted: 10 April 2000

The following members of the CT Scan ARDS Study Group participated in this study: P. Coriat, Department of Anesthesiology, Hôpital de la Pitié-Salpêtrière, Paris, France; Q. Lu, M. O. Roussat, J.-D. Law-Koune, L. Bodin, I. Goldstein, C. Vezinet, Réanimation Chirurgicale Pierre Viars, Hôpital de La Pitié-Salpêtrière, Paris, France; L. Gallart, Servei d'Anestesiologia, Hospital Universitari del Mar, Barcelona, Spain; G. S. Umamaheswara Rao, Department of Anesthesia, National Institute of Mental Health and Neurosciences, Bengalore, India; S. Vieira, Hospital De Clinicas de Porto Allegre, UFRGS, Brazil; L. Malbouisson, Department of Anesthesiology, Hospital Das Clinicas, Sao Paulo, Brazil.

Réanimation Chirurgicale Pierre Viars, Department of Anesthesiology, and the Department of Radiology, Hôpital de la Pitié-Salpêtrière, University of Paris VI and Institut National des Télécommunications, Evry, France
e-mail: louis.puybasset@psl.ap-hop-paris.fr
jean-jacques.rouby@psl.ap-hop-paris.fr
Tel.: + 33-1-42 17 73 00
Fax: + 33-1-42 17 73 26

Correspondence address: L. Puybasset or J.-J. Rouby
Department of Anaesthesiology
Hopital Pitié-Salpetrière
43-83, Boulevard de l'Hopital
75013 Paris-France

Abstract *Objective*: To compare the computed tomographic (CT) analysis of the distribution of gas and tissue in the lungs of patients with ARDS with that in healthy volunteers. *Design:* Prospective study over a 53-month period. *Setting:* Fourteen-bed surgical intensive care unit of a university hospital. *Patients and participants:* Seventy-one consecutive patients with early ARDS and 11 healthy volunteers. *Measurements and results:* A lung CT was performed at end-expiration in patients with ARDS (at zero PEEP) and healthy volunteers. In patients with ARDS, end-expiratory lung volume (gas + tissue) and functional residual capacity (FRC) were reduced by 17 % and 58 % respectively, and an excess lung tissue of 701 ± 321 ml was observed. The loss of gas was more pronounced in the lower than in the upper lobes. The lower lobes of 27 % of the patients were characterized by "compression atelectasis," defined as a massive loss of aeration with no concomitant excess in lung tissue, and "inflammatory atelectasis," defined as a massive loss of aeration associated with an excess lung tissue, was observed in 73 % of the patients. Three groups of patients were differentiated according to the appearance of their CT: 23 % had diffuse attenuations evenly distributed in the two lungs, 36 % had lobar attenuations predominating in the lower lobes, and 41 % had patchy attenuations unevenly distributed in the two lungs. The three groups were similar regarding excess lung tissue in the upper and lower lobes and reduction in FRC in the lower lobes. In contrast, the FRC of the upper lobes was markedly lower in patients with diffuse or patchy attenuations than in healthy volunteers or patients with lobar attenuations. *Conclusions:* These results demonstrate that striking differences in lung morphology, corresponding to different distributions of gas within the lungs, are observed in patients whose respiratory condition fulfills the definition criteria of ARDS.

Key words Computed tomography · Lung morphology · Functional residual capacity · Acute respiratory distress syndrome

Introduction

As recommended by the American-European Consensus Conference of 1994 [1], acute respiratory distress syndrome (ARDS) is defined as the rapid onset of arterial oxygenation impairment together with the appearance of bilateral infiltrates on the frontal chest radiography [2]. Based on these criteria, several hundreds of pa-

tients have recently been included in multicenter randomized studies aimed at evaluating the effects of new therapeutic modalities on the mortality of patients with ARDS. All of these except one [3] have yielded negative results [4, 5, 6, 7, 8]. One possible hypothesis to explain these disappointing results is that the criteria defining ARDS were too imprecise and resulted in the inclusion of patients with heterogeneous lung diseases and thus obscured the beneficial effects of some of these therapies that could have been confirmed in a more homogeneous subgroup of patients. Such heterogeneity is suggested by the clinical observation that patients fulfilling the criteria of the American-European Consensus Conference may have markedly different computed tomographic (CT) appearance.

Lung CT became available in the critical care environment in the middle 1980s, enabling an understanding of the distribution of gas and tissue within the lung parenchyma of patients suffering from ARDS [9]. However, the first generation of CT scanners allowed only a limited assessment of the lung parenchyma because of the long time necessary for acquiring each CT section. A maximum of three CT sections could be analyzed, and these were presumed to be representative of the entire lung [10, 11, 12, 13, 14, 15, 16]. The development of a new generation of fast spiral CT scanners over the past 5 years has overcome this limitation, providing the possibility of visualizing morphological alterations that characterize the entire lung parenchyma of patients with ARDS. In 1992 fast spiral CT became available in our intensive care environment, and we soon observed totally different lung morphologies among patients fulfilling the criteria for ARDS and hypothesized that these differences would have relevant therapeutic implications. Therefore from 1993 to 1997 we performed a prospective study in a large series of patients with ARDS to assess the distribution of gas and tissue within the lungs and to classify the various patterns of lung morphology characterizing ARDS. All images were recorded on optical disks and analyzed in 1998 when a software (Lungview) became available for automatically assessing lung attenuation histograms, lung volumes, and regional distribution of gas and tissue within the overall lung parenchyma.

Methods

Patients

This prospective study was carried out among patients admitted to the Surgical Intensive Care Unit of la Pitié-Salpêtrière Hospital from February 1993 to July 1997 and included 71 consecutive patients with early ARDS for whom there was a delay of less than 10 days between the onset of ARDS and inclusion in the study. Of the 71 patients included in the study 59 were men and 12 were women, with mean age of 56 ± 17 years, height 173 ± 8 cm, and weight 81 ± 14 kg. Admission followed major surgery in 46 patients, multiple trauma in 20, and acute medical illness in 5. ARDS was considered as primary in 49 patients (bronchopneumonia 35, pulmonary contusion 7, aspiration 7), secondary in 20 (extracorporeal circulation 4, intra-abdominal sepsis 1, extra-abdominal sepsis 15), and potentially of both origins in two. Overall mortality was 51%. The mean Lung Injury Severity Score was 2.9 ± 0.6.

ARDS was defined according to the American-European Consensus Conference on ARDS held in 1994 [1]. Inclusion criteria were: (a) PaO_2 less than 200 mmHg at FIO_2 of 1 and zero end-expiratory pressure (ZEEP), (b) bilateral hyperattenuated areas on bedside chest radiography, and (c) pulmonary capillary wedge pressure less than 18 mmHg and/or left ventricular ejection fraction greater than 50% as assessed by transesophageal echocardiography. Each patient with ARDS admitted to our intensive care unit within the study period (1993–1997) underwent a specifically developed therapeutic strategy including thoracic CT under ZEEP and PEEP conditions as well as an investigation of the cardiorespiratory effects of inhaled nitric oxide, intravenous almitrine, and expiratory washout in subgroups of patients. All therapeutic as well as investigational procedures were approved by the local ethics committee. In all cases written informed consent was obtained from the patient's next of kin. Partial results concerning the CT data of some patients have been reported in previous studies [17, 18, 19, 20, 21]. However, Lungview was not available at that time, and the CT of each concerned patient was entirely reanalyzed for the present study.

Protocol

Throughout the study period all patients were sedated and paralyzed with fentanyl, midazolam, and vecuronium. Patients were ventilated using controlled mechanical ventilation (César Ventilator, Taema, France) to achieve $PaCO_2$ values between 30 and 50 mmHg. An inspiratory time of 33% and a FIO_2 of 1 were maintained throughout the study period. All patients were monitored using Swan-Ganz and arterial catheters. The study itself consisted of hemodynamic, respiratory, and lung mechanics and of CT measurements performed in ZEEP and after implementation of a PEEP of 10 cmH_2O.

Spiral thoracic CT was also performed at end-expiration in 11 spontaneously breathing healthy volunteers to determine the normal values of lung volumes of gas and tissue (9 men, 2 women; mean age 35 ± 10 years, height 171 ± 6 cm, weight 67 ± 10 kg). Each healthy volunteer was an investigator of the present study (author or member of the CT Scan ARDS Study Group) and provided a written informed consent. The present article constitutes part 1 of the overall study and reports the results obtained in ZEEP. Part 2 [22] addresses the morphophysiological correlations and part 3 [23] the effects of PEEP.

High-resolution and spiral thoracic CT

Acquisition of CT

Each patient was transported to the Department of Radiology by two physicians. Mechanical ventilation was provided using an Osiris ventilator (Taema, France) delivering 100% oxygen. Electrocardiography, pulse oxymetry, and systemic arterial pressure were monitored continuously using a Propaq 104 EL monitor (Protocol System, North Chicago, Ill., USA). The 15-s apnea necessary to obtain the CT sections in ZEEP resulted in a transient desaturation in

most patients. However, the lowest oxygen saturation measured was 85%. In the supine position, lung scanning was performed from the apex to the diaphragm using a Tomoscan SR 7000 (Philips, Eindhoven, The Netherlands) as previously described [17, 18, 19, 20, 21]. All images were observed and photographed at a window width of 1600 HU and a level of –600 HU. The exposures were taken at 120 kV and 250 mA. The value of the pitch was 1. An intravenous injection of 80 ml contrast medium was used to differentiate pleural effusions from nonaerated lung parenchyma. Evaluation included thin and spiral CT sections. The thin-section CT examination consisted of a series of 1.5-mm sections with 20-mm intersection spacing selected by means of a thoracic scout view during a 15-s apnea. For spiral CT, contiguous axial sections 10-mm thick were reconstructed from the volumetric data. One set of thin and spiral sections was obtained at end-expiration in ZEEP, the patient being disconnected from the ventilator and a second set at PEEP of 10 cmH_2O. All CT sections were recorded on an optical disk for later computerized analysis.

In healthy volunteers the same technical procedure was followed as in patients except that CT sections were obtained at end-expiration without PEEP. The results concerning the healthy volunteers have been partially reported in two recent studies [19, 20].

Classification according to lung morphology at CT

Each patient was classified by an independent radiologist (P.C.) unaware of the clinical conditions of the patient on the basis of the distribution of CT attenuations. According to the Fleischner Society Nomenclature Committee [24], CT attenuations included CT consolidations and ground-glass opacification. Consolidation was defined as a homogeneous increase in pulmonary parenchymal attenuation that obscures the margins of the vessels and airway walls. Ground-glass opacities were defined as hazy, increased attenuations of lung but with preservation of bronchial and vascular margins. The two entities may be associated with an air bronchogram. The patient was classified as having a *lobar* pattern if areas of lung attenuation had a lobar or segmental distribution established on the recognition of anatomical structures such as the major fissura or the interlobular septa, a *diffuse* pattern if lung attenuations were diffusely distributed throughout the lungs, and a *patchy* pattern if there were lobar or segmental areas of lung attenuation in some parts of the lungs but lung attenuations without recognized anatomical limits in others. The interobserver variability with this method of classification was assessed by counting misclassifications between a first and a second radiologist (P.C.); intraobserver variability was assessed by counting misclassifications between two different evaluations performed by the same observer. All CT images were reviewed: 2 patients were classified differently by the two radiologists while only one was classified differently by the same observer on the second evaluation.

Analysis of the distribution of hyperattenuated areas within the pulmonary segments

The distribution of radiologically hyperattenuated areas on the CT within the 18 pulmonary segments was analyzed by the radiologist according to a previously described semiquantitative technique [17]. Briefly, pleural effusions and hilar and mediastinal structures were delineated, and thin sections were used to identify fissures and anatomical bronchovascular structures. Systematic anatomical marking of the 5 pulmonary lobes and 18 pulmonary segments was then performed by studying the relationship between bronchi, arteries, veins, fissures, and surrounding lung parenchyma [25]. The percentage of nonaerated lung parenchyma in each pulmonary segment was assessed visually.

Measurement of lung dimensions and of the volumes of gas and tissue

The cephalocaudal dimension of each lung was determined as the number of 10-mm-thick sections present between the lung apex and the dome of the diaphragmatic cupola. On each CT section six regions of interest (the right and left upper and the lower lobes, right and left pleural effusions) were delineated using the roller ball of the computer after the right and left lung outlines and the position of the major fissura had been identified. Areas of maximal size within the defined anatomical limits were outlined to include as much of the lung as possible. To maintain the symmetry between right and left lungs, the right middle lobe was considered as a part of the right upper lobe. For each region of interest the end-expiratory lung volume (gas + tissue), the respective volumes of gas and tissue, and the distribution of lung aeration were quantified using a specially designed software, Lungview (Institut National des Telecommunications, Evry, France). For technical reasons (lost and unreadable optical disks), this analysis was performed only in 48 of the 71 patients initially included (60% of those with lobar attenuations, 82% of those with diffuse attenuations, and 66% of those with patchy attenuations). Of these, 36% had lobar attenuations, 23% diffuse attenuations, and 41% patchy attenuations.

Using Lungview, the lung volume was computed as the total number of voxels present in a given region of interest times the volume of the voxel. The respective volumes of gas and tissue were measured using a method previously described [11, 19, 21] and based on the close correlation between CT attenuation (expressed as the CT number) and physical density [26]. The CT number characterizing each individual voxel is expressed in Hounsfield units (HU) and is defined as the attenuation coefficient of the X-ray by the material being studied minus the attenuation coefficient of water divided by the attenuation coefficient of water. By convention, the CT number of water is 0 (HU) and lung tissue was assumed to have a density very close to the density of water. The CT number is scaled by a factor 1000, the CT number of gas being –1000 HU. A lung area characterized by a mean CT number of –500 HU is considered as being composed of 50% of gas and 50% of tissue. A lung area characterized by a mean CT number of –200 HU is considered as being composed of 20% of gas and 80% of tissue. In a first step, the distribution of lung attenuations was measured on each CT section for 256 compartments between –1200 HU and + 200 HU, examining an interval of 5.47 HU. Each compartment was composed of voxels characterized by CT numbers ranging in an interval of 5.47 HU. For each compartment of a known number of voxels, the total volume, the volume of gas and tissue, and the fraction of gas were computed using the following equations:

$$\text{Volume of the voxel} = (\text{size of the pixel})^2 \times \text{section thickness} \quad (1)$$

$$\text{Total volume} = \text{number of voxels} \times \text{volume of the voxel} \quad (2)$$

$$\text{Volume of gas} = (-\text{CT}/1000) \times \text{total volume if the compartment considered has a CT number below 0 (volume of gas = 0 if the compartment considered has a CT number above 0)} \quad (3)$$

$$\text{Volume of tissue} = (1 + \text{CT}/1000) \times \text{total volume if the compartment considered has a CT number below 0 or} \quad (4)$$

Volume of tissue = number of voxels × volume of the voxel if the compartment considered has a CT number above 0 (4′)

Fraction of gas = volume of gas/total volume (5)

where CT is the mean CT number of the compartment analyzed.

In a second step, the volumes of gas and tissue of each region of interest were calculated by adding the values of all the compartments present within the region of interest. In a third step, the volumes of gas and tissue of the overall lung were calculated by adding the volumes of the four regions of interest of the lungs (right upper and lower lobes + left upper and lower lobes). The overall lung volume at end-expiration (gas + tissue) was defined as end-expiratory lung volume. The overall volume of gas present in both lungs at end-expiration was defined as functional residual capacity (FRC).

The measurements of the volumes of gas and tissue using Lungview were validated by performing CT of five 2.3-l reservoirs filled with different, known volumes of gas and water emulsified with soap. To measure gas volume the mean bias and precision using the method of Bland and Altman [27] were 3 and 25 ml. The equation of the linear regression was: volume of gas = 1.006 × actual volume + 22 ml, $r = 1$. As far as the measurement of water volume, the mean bias and precision were –2 and 33 ml. The equation of the linear regression was: volume of water = 0.97 × actual volume + 40 ml, $r = 1$.

Reproducibility was assessed in three of the investigators by acquiring two CT scans at intervals of a few weeks. The mean difference between the two measurements was 107 ml for the end-expiratory lung volume, 56 ml for FRC, and 50 ml for the volume of tissue.

Measurement of lung volumes with different degree of aeration

To differentiate the lung zones with different degrees of aeration the entire lung was divided into four zones as previously described: lung zones with a CT number between –1000 and –900 HU were considered as overdistended [19], those between –900 and –500 HU as normally aerated [10, 19], those between –500 and –100 HU as poorly aerated, and those between –100 and + 100 HU as nonaerated [10]. Nonaerated lung regions were considered as atelectatic regions and divided into two separate entities. "Compression atelectasis" was defined as a nonaerated lung region without excess tissue, and "inflammatory atelectasis" as a nonaerated lung region with concomitant excess lung tissue. Excess tissue was defined as a volume of tissue greater than the mean volume of tissue measured in healthy volunteers plus 1 SD.

Bedside chest radiograph

Bedside frontal chest radiography was performed within 12 h of the CT. Lung parenchyma was divided into four quadrants by a vertical mediastinal line and an horizontal hilar line as proposed by Murray et al. [2]. The presence of hyperattenuated areas in each of the quarters and the obliteration of the left or right diaphragmatic cupola were analyzed by an independent radiologist (P. C.).

Statistical Analysis

Comparisons between groups were performed by a one-way analysis of variance for one grouping factor followed by Fisher's probabilistic least significant difference post hoc comparison test for continuous variables and by the χ^2 test for discontinuous variables. Comparisons between the upper and lower lobes were analyzed by a two-way analysis of variance for two grouping factors. Data in the text and tables are presented as mean ± SD. The statistical analyses were performed using Statview 4.0.2 and SuperANOVA statistical software (Abacus Concepts, Berkeley, Calif., USA). The level of statistical significance was set at $p \leq 0.05$.

Results

End-expiratory lung volumes and FRC in healthy volunteers and in patients with ARDS

In healthy volunteers the upper lobes accounted for 54 ± 4 % of the end-expiratory lung volume and the right lung for 53 ± 2 %. As shown in Fig. 1 and Table 1, the FRC of the upper lobes was higher than that of the lower lobes, while the volume of lung tissue was similar in the upper and lower lobes.

As compared to healthy volunteers, the end-expiratory lung volume of patients with ARDS was significantly reduced by 17 % and volume loss was essentially related to a reduction in the volume of the lower lobes (Table 1). As shown in Fig. 1, the cephalocaudal dimensions of the right and left lungs were significantly reduced, and in the same proportion in the three groups of patients. As shown in Fig. 2, patients with ARDS had a greater amount of lung tissue than healthy volunteers that was more pronounced in the upper than in the lower lobes (+ 97 % vs. + 53 %; $p < 0.0001$). Each patient had lung tissue in excess at the level of the upper lobes, but only 35 of the 48 patients studied (73 %) had lung tissue in excess in their lower lobes. As shown in Fig. 1, there was a significantly lower FRC in patients than in healthy volunteers, particularly in the lower lobes (–84 % in the lower lobes vs. –38 % in the upper lobes; $p < 0.0001$).

Morphological differences between the respective groups

Differences in bedside chest radiography

In patients with lobar attenuations, hyperattenuated areas were bilateral and located predominantly in the lower quadrants. Because hyperattenuated lung areas were sparse and less frequent in the upper lobes, which remained essentially aerated, the first clinical impression at the bedside was a lack of extensive radiological lesions, in contrast to the severity of arterial oxygenation impairment (Fig. 3 a). In contrast, patients with diffuse or patchy attenuations had radiological attenuations involving all pulmonary quadrants, obliterating mediastinal borders and less frequently diaphragmatic cupola. The loss of aeration involved the entire lung parenchyma and gave the immediate visual impression of radio-

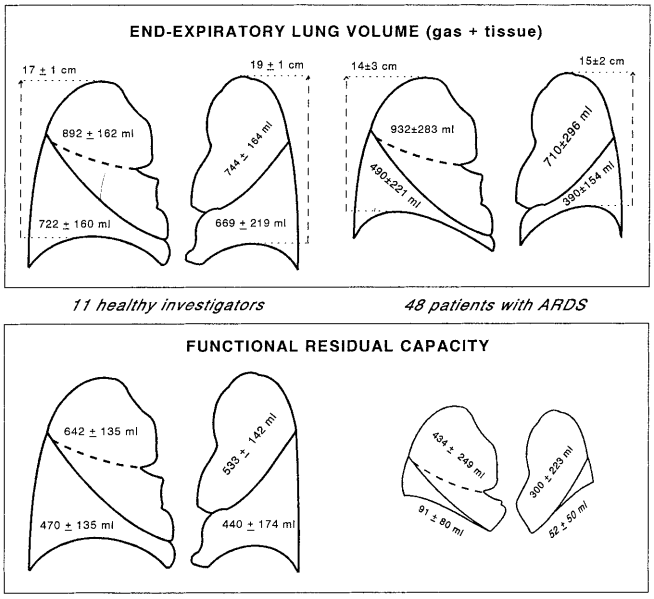

Fig. 1 End-expiratory lung volumes and functional residual capacity of the upper and lower lobes in 11 healthy volunteers and 48 patients with ARDS. Both lungs are presented in a lateral view, allowing the representation of the main fissura, the upper lobes, and the lower lobes. The cephalocaudal dimensions of the lungs are represented in centimeters (*vertical dashed line*). Data are presented as mean ± SD

logical severity, with the classical aspect of "white lungs" (Fig. 3b, c). Figure 4 presents the distribution of radiologically hyperattenuated lung areas and incidence of the obliteration of right and left diaphragmatic cupola in the three groups.

Differences in distribution of gas and tissue

Hyperattenuated lung areas were observed almost exclusively in the lower lobes in patients with lobar attenuations (Fig. 5). In contrast, hyperattenuated lung areas were distributed uniformly, involving all pulmonary segments in patients with diffuse attenuations. The segmental distribution of the hyperattenuated lung areas of patients with patchy attenuations involved all pulmonary segments but predominated in the lower lobes. Figures 6, 7, and 8 present the CT of the three patients whose bedside chest radiographs are displayed in Fig. 3.

The volumic distribution of CT attenuations in patients with lobar attenuations was bimodal, corresponding to a coexistence of normally aerated and nonaerated lung regions (Fig. 9). On the other hand, the volumic distribution of CT attenuations in patients with diffuse attenuations was unimodal, corresponding to a predominance of poorly and nonaerated lung regions. Patients with patchy attenuations showed an intermediate pattern.

CT attenuation histograms characterizing the lower lobes were unimodal and very similar in the three groups (Fig. 10), corresponding to a predominance of nonaerated lung regions (Table 2). In contrast, CT attenuation histograms characterizing the upper lobes were unimodal in patients with diffuse attenuations, corresponding to a predominance of nonaerated lung regions, and bimodal in patients with lobar attenuations and patchy attenuations, corresponding to a coexistence of normally aerated and nonaerated regions (Table 2).

The distribution within lower lobes of normally, poorly, and nonaerated lung volumes was similar in the three groups, with a massive predominance of poorly

Table 1 Volumes of gas and tissue in healthy volunteers and patients with ARDS [End-expiratory lung volume = total lung volume (gas + tissue); *LA* lobar attenuations, *DA* diffuse attenuations, *PA* patchy attenuations]

		Patients with ARDS (n = 48)		
	Volunteers (n = 11)	LA (n = 15)	DA (n = 14)	PA (n = 19)
Total lung				
Pleural fluid (ml)	0 ± 0	293 ± 271*	250 ± 229*	319 ± 406*
End-expiratory lung volume (ml)	3028 ± 637	2860 ± 626	2362 ± 604*,**	2373 ± 686*,**
FRC (ml)	2085 ± 537	1314 ± 394*	553 ± 237*,**	773 ± 326*,**,***
Volume of tissue (ml)	943 ± 143	1546 ± 368*	1809 ± 477*	1600 ± 450*
Fraction of gas (%)	69 ± 4	46 ± 8*	23 ± 8*,**	32 ± 9*,**,***
Upper lobes				
End-expiratory lung volume (ml)	1636 ± 319	2037 ± 562	1413 ± 369	1501 ± 435
FRC (ml)	1175 ± 273	1184 ± 376	389 ± 169*	635 ± 287*
Volume of tissue (ml)	461 ± 68	853 ± 244*	1024 ± 296*	866 ± 220*
Fraction of gas (%)	72 ± 4	58 ± 7*	28 ± 10*,**	40 ± 11*,**,***
Lower lobes				
End-expiratory lung volume (ml)	1391 ± 367	823 ± 286*	949 ± 295*	872 ± 353*
FRC (ml)	909 ± 299	131 ± 103*	164 ± 111*	138 ± 87*
Volume of tissue (ml)	482 ± 89	693 ± 238*	785 ± 227*	734 ± 282*
Fraction of gas (%)	65 ± 5	16 ± 10*	17 ± 9*	15 ± 7*

*$p < 0.01$ vs. healthy volunteers, **$p < 0.05$ vs. patients with lobar attenuations, ***$p < 0.05$vs. patients with diffuse attenuations

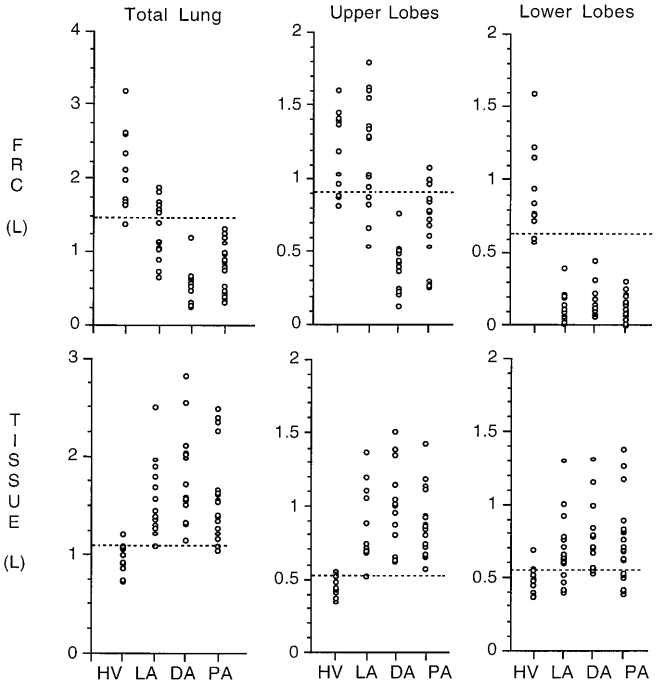

Fig. 2 Functional residual capacity (FRC) and volume of lung tissue measured in both lungs overall, in the upper lobes, and in the lower lobes in each patient with ARDS and in each healthy volunteer (*HV*). *LA* Lobar attenuations; *DA* diffuse attenuations; *PA* patchy attenuations; *dashed lines* upper normal limit of FRC and the lower normal limit of lung tissue calculated as the mean value observed in healthy volunteers ± 1 SD

and nonaerated lung regions. In contrast, the distribution of normally, poorly, and nonaerated lung volumes within the upper lobes differed between the three groups. In patients with lobar attenuations, normally aerated lung regions were more frequent than poorly or nonaerated lung regions. In patients with diffuse attenuations, poorly and nonaerated lung regions were more frequent than normally aerated lung regions. Patients with patchy attenuations showed an intermediate pattern.

Differences in end-expiratory lung volume and FRC

As shown in Table 1, end-expiratory lung volume was significantly lower in patients with diffuse and patchy attenuations than in healthy volunteers. In contrast, end-expiratory lung volume remained unchanged in patients with lobar attenuations because the decrease in FRC, predominating in lower lobes, was compensated by an

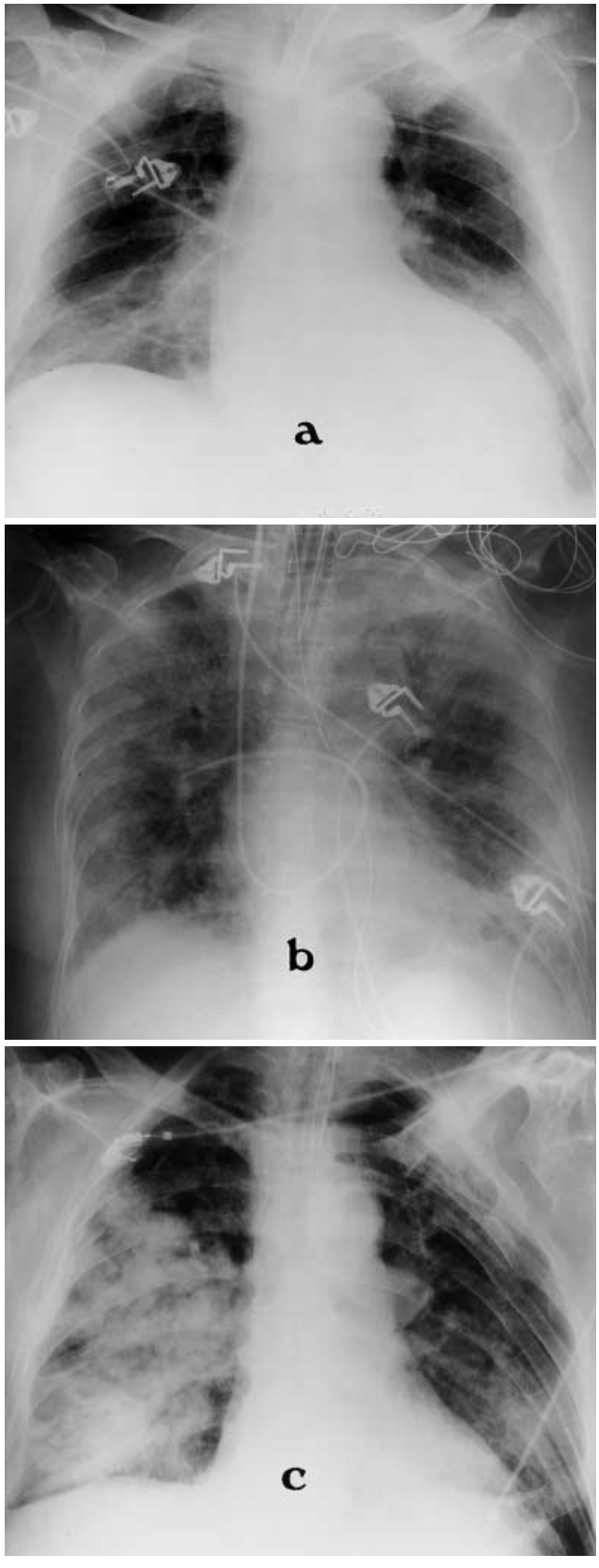

Fig. 3 Bedside chest radiograph of three different patients with lobar (**a**), diffuse (**b**), and patchy attenuations (**c**)

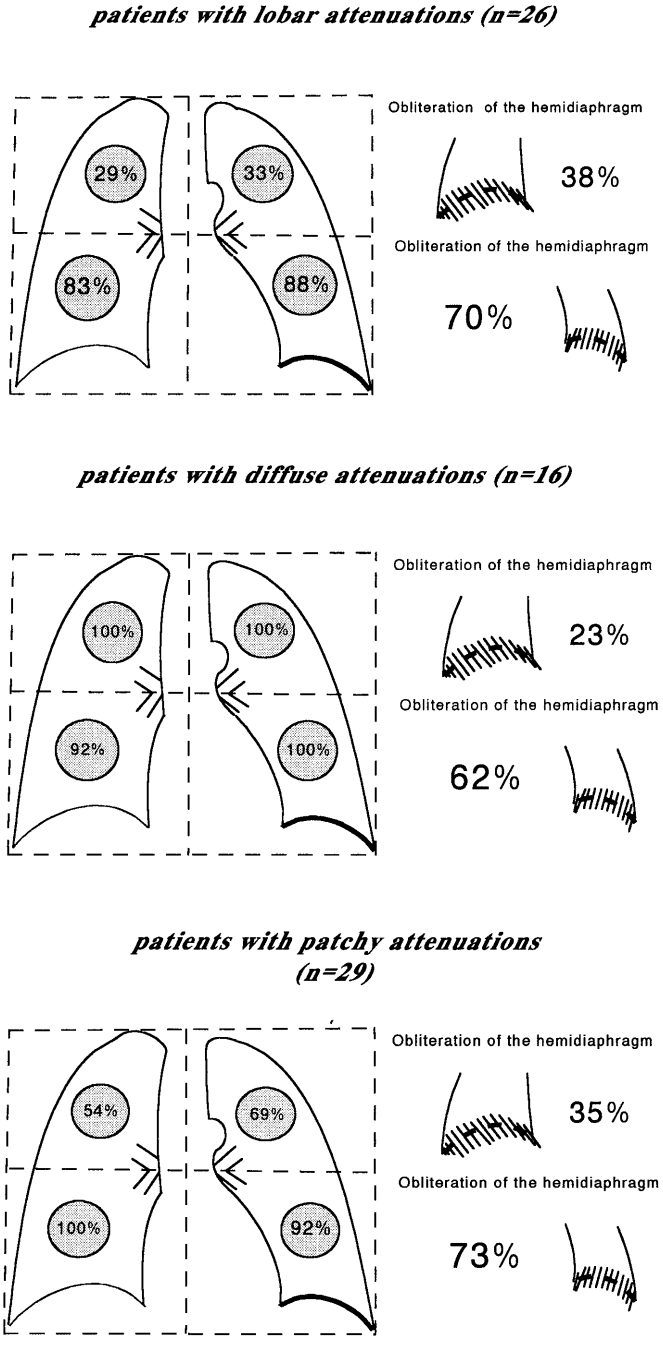

Fig. 4 Distribution of radiological hyperattenuated lung areas and incidence of the obliteration of the diaphragmatic cupola in the 71 patients with ARDS. *Encircled numbers* Percentage of patients of each group having hyperattenuated lung areas in the quadrant considered; *right* percentage of patients having an obliteration of the right and left diaphragmatic cupola

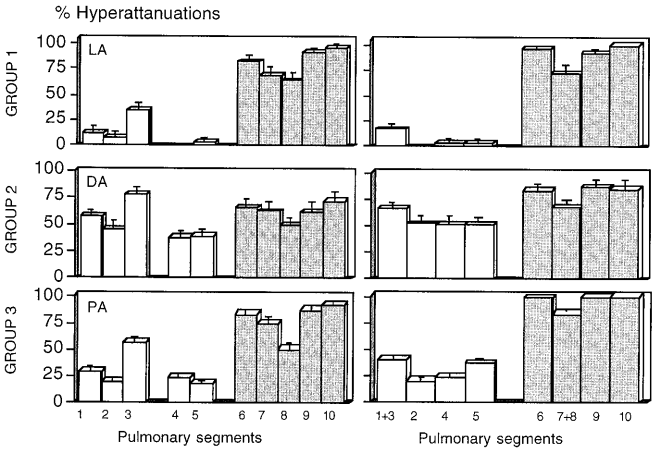

Fig. 5 Percentage of each pulmonary segment of the right (*left*) and left lungs (*right*) characterized by CT hyperattenuations in patients with lobar attenuations (*LA*, *group 1*, *upper*), diffuse attenuations (*DA*, *group 2*, *middle*), and patchy attenuations (*PA*, *group 3*, *lower*). *X-axis* Anatomical numeration of pulmonary segments. Data are mean ± SEM

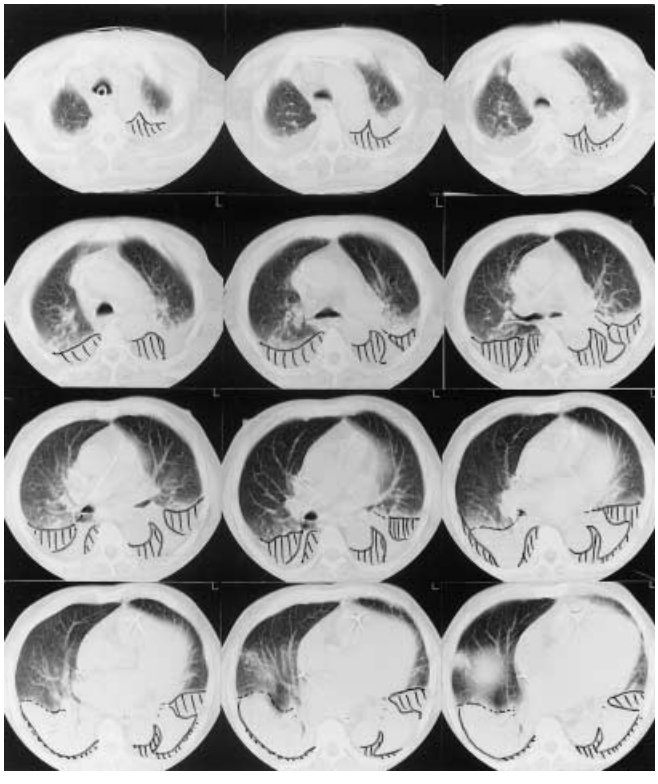

Fig. 6 Representative CT of a patient with lobar attenuations. *Dashed line* Position of the major fissura; *hatched areas* pleural effusion. The functional residual capacity was 1555 ml and 6 ml in the upper and lower lobes, respectively. The volume of tissue was 1375 and 423 ml in the upper and lower lobes, respectively. The amount of pleural effusion was 485 ml

Fig. 7 Representative CT of a patient with diffuse attenuations. *Dashed line* Position of the major fissura; *hatched areas* pleural effusion. The functional residual capacity was 365 ml and 107 ml in the upper and lower lobes, respectively. The volume of tissue was 1010 and 707 ml in the upper and lower lobes, respectively. The amount of pleural effusion was 606 ml

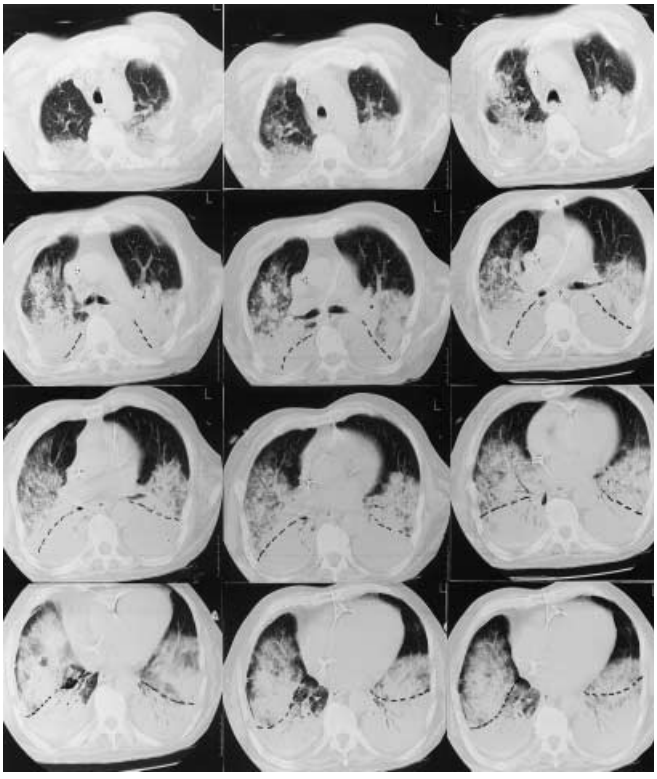

Fig. 8 Representative CT of a patient with patchy attenuations. *Dashed line* Position of the major fissura. The functional residual capacity was 861 ml in the upper lobes and 35 ml and lower lobes. The volume of tissue was 1430 ml in the upper lobes and 861 ml in lower lobes

equivalent amount of excess tissue in the upper and lower lobes.

The end-expiratory lung volume of the lower lobes was lower in all three groups of patients than in healthy volunteers (Table 1), but that in the upper lobes remained unchanged. The excess lung tissue, present in all patients, and its distribution between the upper and lower lobes did not differ between the three groups.

In patients with lobar attenuations FRC of the upper lobes did not differ significantly from that in healthy volunteers, but it was markedly reduced in patients with diffuse or patchy attenuations. The radiological appearance of the upper lobes was affected mainly by the loss of aeration and not by the excess in lung tissue. Figures 6, 7, and 11 illustrate this finding by showing patients with similar excess in lung tissue in their upper lobes but totally different radiological presentations. In contrast, the radiological appearance of the lower lobes was similar between the three groups and characterized by a dramatic loss of aeration. In each group there were some patients who were free of any excess lung tissue in their lower lobes, suggesting that the dramatic loss of aeration was related to "compression atelectasis" (loss of air associated with a normal amount of lung tissue). Such a passive atelectasis characterizing the lower lobes had a similar prevalence in the three groups (27 % with lobar attenuations, 32 % with patchy attenuations, and 21 % with diffuse attenuations; NS).

Discussion

This study demonstrates that ARDS is characterized morphologically by a marked excess in lung tissue associated with a major reduction in FRC. However, because the loss of gas is greater than the excess lung tissue, the end-expiratory lung volume decreases. Although more pronounced in the upper lobes, the excess lung tissue is disseminated in the upper and lower lobes. "Inflammatory atelectasis " – loss of gas plus excess lung tissue – or "compression atelectasis " – loss of gas without excess lung tissue – is always present in the lower lobes but only occasionally in the upper lobes. An up-

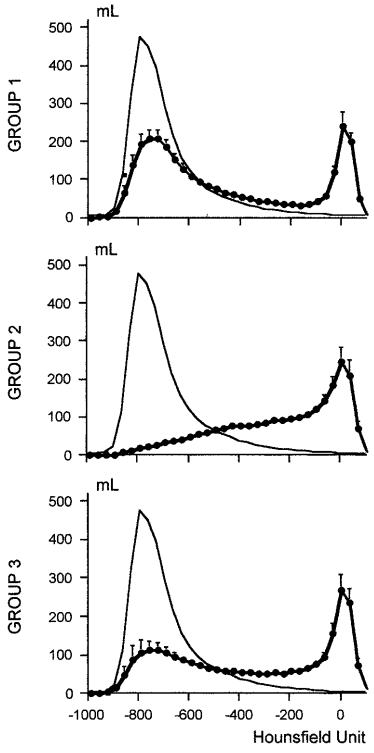

Fig. 9 Volumic distribution of CT attenuations in the three groups of patients in ZEEP conditions: lobar attenuations (*group 1*, *upper*), diffuse attenuations (*group 2*, *middle*), patchy attenuations (*group 3*, *lower*). *Y-axis* Lung volume represented as the number of voxels corresponding to different CT attenuations (*X-axis*). *Light line* CT attenuation histograms of the healthy volunteers. To improve readability, each value represents the volume of six consecutive intervals of 5.47 HU. Data are mean ± SEM

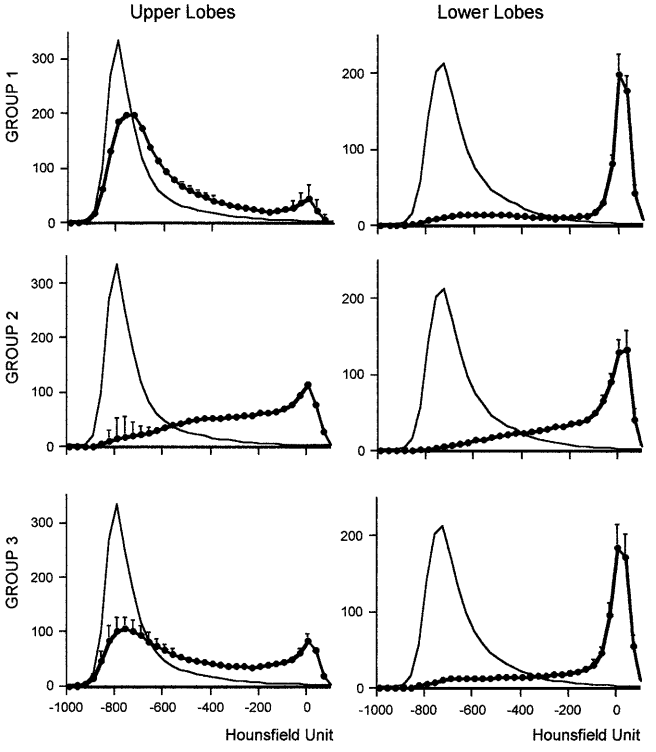

Fig. 10 Volumic distribution of CT attenuations in the the upper (*left*) and lower lobes (*right*) of the three groups of patients in ZEEP conditions: lobar attenuations (*group 1*, *upper*), diffuse attenuations (*group 2*, *middle*), patchy attenuations (*group 3*, *lower*). *Y-axis* Lung volume represented as the number of voxels corresponding to different CT attenuations (*X-axis*). *Light line* CT attenuation histograms of the healthy volunteers. To improve readability, each value represents the volume of six consecutive intervals of 5.47 HU. Data are mean ± SEM

ward shift of the diaphragm and increase in lung weight are likely factors that mechanically compress the lower lobes, explaining why they appear as essentially nonaerated in every patient with ARDS. In contrast, many of these patients have a preservation of the aeration of their upper lobes despite a marked excess in lung tissue. Accordingly, their chest radiograph appears relatively well aerated and quite different from that of patients with the same excess lung tissue but in whom there is a massive loss of gas in the upper lobes and who typically demonstrate "white lungs." These results demonstrate that striking differences in lung morphology, corresponding to different distributions of gas within the diseased lungs, are observed in patients whose respiratory condition fulfills the criteria of lung ARDS.

Methodological considerations

In the present study we used a specially designed software (Lungview) to assess lung volumes and distribution of gas and tissue within the lungs. Its accuracy was assessed by scanning large reservoirs containing a soapy emulsion obtained from known volumes of water, soap, and air. To date, FRC has been measured mainly in ARDS by nitrogen [28] or sulfur hexafluoride washout [9, 29] and open and closed circuit helium dilution techniques [28, 30]. These methods have the advantage of being noninvasive and thus allowing repeated bedside measurements. However, their accuracy and reproducibility are limited by technical problems such as changes in gas viscosity during the washout maneuver [31]. In addition, they cannot detect gas trapped behind completely or nearly closed airways. As a consequence CT assessment of FRC may represent an attractive alternative to these techniques.

The CT approach also allows a qualitative assessment of the distribution of gas and lung tissue within a given pulmonary structure. Four different lung compartments can be defined according to their lung attenuation: overdistended lung areas (–1000 to –900 HU) are not normally present in healthy volunteers [19] and are

Table 2 Overdistended, normally, poorly, and nonaerated lung volumes (ml) in healthy volunteers and patients with ARDS (*LA* lobar attenuations, *DA* diffuse attenuations, *PA* patchy attenuations)

		Patients with ARDS (n = 48)		
	Volunteers (n = 11)	LA (n = 15)	DA (n = 14)	PA (n = 19)
Total				
Overdistended lung	3 ± 5	3 ± 5	1 ± 3	4 ± 9
Normally aerated lung	2709 ± 684	1590 ± 498*	367 ± 262*,**	806 ± 435*,**,***
Poorly aerated lung	302 ± 135	555 ± 170*	1025 ± 345*,**	703 ± 240*,***
Nonaerated lung	15 ± 5	712 ± 300*	968 ± 373*	860 ± 340*
Upper lobes				
Overdistended lung	2 ± 4	3 ± 5	1 ± 2	4 ± 9
Normally aerated lung	1505 ± 322	1468 ± 481	275 ± 188*,**	698 ± 387*,**,***
Poorly aerated lung	123 ± 41	406 ± 162*	676 ± 245*	489 ± 164*
Nonaerated lung	6 ± 3	160 ± 140*	460 ± 255*	299 ± 171*
Lower lobes				
Overdistended lung	0 ± 1	0 ± 0	0 ± 0	0 ± 1
Normally aerated lung	1204 ± 408	122 ± 117*	92 ± 104*	108 ± 88*
Poorly aerated lung	178 ± 101	149 ± 105	349 ± 201*,**	214 ± 139***
Nonaerated lung	8 ± 3	552 ± 200*	508 ± 184*	550 ± 218*

*$p < 0.05$ vs. healthy volunteers, **$p < 0.05$ vs. patients with lobar attenuations, ***$p < 0.05$ vs. patients with diffuse attenuations

found in patients with emphysema bullae [32]; normally aerated lung areas (–900 to –500 HU) represent more than 95 % of the normal lung parenchyma [10, 19]; poorly and nonaerated lung areas (–500 to –100 HU and above –100 HU) are found only in patients with acute or chronic lung injury. Another advantage of the CT approach is that the upper and lower lobes can be separately analyzed after the manual delineation of main fissures. It must be pointed out that this delineation can be difficult when hyperattenuated lung areas and loss of gas involve both upper and lower lobes.

Histologically, the injured lung is characterized by an excessive amount of extravascular lung water and by an infiltration of lung structures by inflammatory cells. Edema and inflammation are indistinguishable on the CT and are measured by Lungview as "excess tissue." One important limitation of CT is its inability to distinguish between increased intrapulmonary blood and excess lung inflammation. In contrast, a software such as Lungview allows the differentiation of "compression atelectasis," characterized by a loss of aeration without excess lung tissue, from "inflammatory atelectasis," characterized by a loss of aeration associated with excess lung tissue.

Regional distribution of gas and tissue in healthy volunteers

In healthy volunteers the FRC was 2085 ± 537 ml, close to that (2305 ± 377 ml) computed with the formula of Quanjer et al. [33] for adults lying in supine position. The mean volume of lung tissue was 943 ± 143 ml. This value is similar to that measured by Gattinoni et al. [11] in the late 1980s by combining the helium dilution technique and CT. It can be assumed that intrapulmonary blood accounted for 450 ml and lung structures for the remaining weight [34].

Regional distribution of gas and tissue in patients with ARDS

Overall we found 17 % less end-expiratory lung volume in patients than in healthy volunteers of similar height and body surface area. As described previously [20], the decrease in end-expiratory lung volume is due to the upward shift of the diaphragm, resulting in reduced cephalocaudal dimensions of the lungs and thus explaining the specific reduction in the end-expiratory lung volume of the lower lobes.

The FRC measured in ZEEP conditions was reduced by 58 %. This value is in the range of that previously measured by dilution techniques [35, 36, 37]. The total volume of lung tissue was increased by 74 %, corresponding to an absolute change of 701 ml. Assuming that pulmonary blood pooling is unlikely in ARDS because of the generalized constriction of the pulmonary circulation, it can be hypothesized that this increase in lung tissue volume resulted mainly from the presence of an excess amount of extravascular lung water and inflammatory cells.

Surprinsingly, the excess lung tissue was more pronounced in the upper than in the lower lobes. All patients demonstrated excess lung tissue in the upper lobes, while the volume of lung tissue present in the lower lobes remained in the normal range in 27 % of the patients. In ARDS two factors should tend to promote ac-

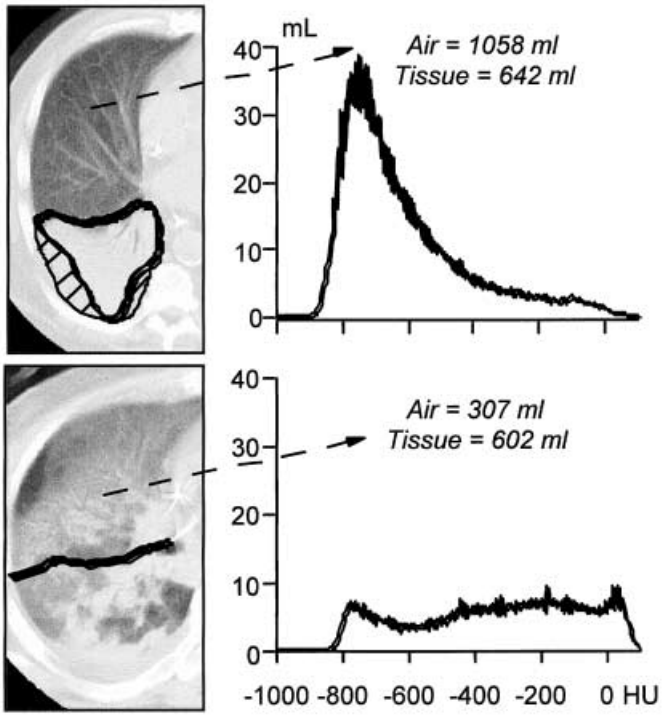

Fig. 11 Illustrative examples of a patient with lobar attenuations (*upper*) and a patient with diffuse attenuations (*lower*). *Left* CT of the right lung; *right* volumic distribution of CT numbers for the upper lobe. The volumes of gas and tissue computed with Lungview are shown above the CT attenuation histogram. The excess lung tissue present in the upper lobes is similar in the two patients. In contrast, there is four times as much gas in the upper lobe of the patient with lobar attenuations than in the upper lobe of the patient with diffuse attenuations. This difference in the fraction of gas markedly affects the CT image, the upper lobe of the patient with lobar attenuations appearing grossly "normal" whereas the upper lobe of the patient with diffuse attenuations appearing "abnormal"

cumulation of lung edema in the lower rather than the upper lobes: the dependent position of the lower lobes in the supine position and the anatomical predominance of the pulmonary vascularization in the lower lobes. One hypothesis to explain the paradoxical predominance of excess lung tissue in the upper lobes is that of a redistribution of pulmonary blood flow towards the upper lobes related to hypoxic pulmonary vasoconstriction occurring in the dependent regions of the lung [38]. Another hypothesis is that the nonhomogeneous distribution of the excess lung tissue truly reflects an uneven distribution of pulmonary edema. Edema formation depends grossly on the transmural microvascular pressure and on the capillary filtration coefficient [39]. In supine position an atelectatic lower lobe might be less prone to generate edema than a nonatelectatic upper lobe despite a higher microvascular pressure; the reduced size of the vessels due to atelectasis could reduce the size of the "holes" present in the alveolocapillary barrier, thereby decreasing the capillary filtration coefficient.

Physiologically, the degree of lung aeration depends on the transpulmonary pressure and the quality of the surfactant. Transpulmonary pressure is subject to anteroposterior and cephalocaudal gradients. The anteroposterior gradient is related to gravity [16, 40] while the cephalocaudal gradient results from the transmission of the abdominal pressure to the thoracic cavity [41, 42]. Physiologically, the most caudal and dependent parts of the lung, i.e., the lower lobes, are subjected to a lower transpulmonary pressure than the most cephalic and nondependent parts of the lung, i.e., the upper lobes. In critically ill patients with ARDS, several factors contribute to exaggerating these physiological gradients: increased lung weight [16], increased abdominal pressure following abdominal surgery or related to acute lung injury, upward shift of the diaphragmatic cupola subsequent to anesthesia and paralysis [43] and increased heart weight [44].

Regional distribution of gas and tissue according to lung morphology

Diffuse attenuations were found in 23 % of patients, and CT attenuations almost exclusively in the lower lobes in 35 %. In 41 % there were patchy attenuations. Each patient fulfilled the clinical and radiological criteria for ARDS at the time of inclusion in the study. The excess in lung tissue was comparable in the three groups of patients, suggesting that the amount of lung inflammation and edema was similar despite the differences in radiological presentation. In fact, only the volume and the distribution of gas differed between the three groups. In patients with diffuse attenuations, lung attenuations histograms showed a unimodal distribution with a predominance of poorly and nonaerated lung areas that represented more than 80 % of the end-expiratory lung volume. Radiologically, this corresponded to bilateral diffuse lung opacities and "ground glass" involving equally the upper and lower lobes. In contrast, patients with lobar attenuations showed a bimodal distribution of lung attenuation histograms with an equal distribution of normally aerated lung areas and poorly or nonaerated lung areas that represented less than 45 % of the end-expiratory lung volume. Radiologically, this corresponded to "white" lower lobes coexisting with "black" upper lobes. Surprisingly, no difference was observed between groups as far as the amount of lung tissue in excess present in the upper lobes. As illustrated in Fig. 11, CT and radiological patterns of the upper lobes of patients with ARDS were affected more by the degree of aeration rather than by the amount of lung tissue in excess. In fact, the only difference between the three groups was the degree of aeration of

the upper lobes, which remained normal in patients with lobar attenuations and was markedly reduced in the other two groups.

In the lower lobes the loss of aeration and increase in lung tissue were identical in the three groups (Fig. 10). No excess in lung tissue was found in the lower lobes in four patients with lobar attenuations, three with diffuse attenuations, and six with patchy attenuations, suggesting that the loss of aeration was related to a "compression atelectasis." This finding argues for the existence of common mechanisms – such as the upward shift of the diaphragm and the increased lung and cardiac weights – exerting a direct mechanical compression on the lower lobes in all patients with ARDS.

Reasons for these differences in lung morphology can only be speculated upon. The main determinants of the regional degree of aeration in ARDS are the regional quality of the surfactant and the local transpulmonary pressure. It is highly likely that deep sedation and muscle paralysis and increased abdominal pressure and heart weight contribute in every patient with ARDS to a significant decrease in the transpulmonary pressure in caudal lung regions, thereby explaining the massive atelectasis of the lower lobes. In contrast, it can be assumed that the transpulmonary pressure in cephalic lung region is preserved because the increase in abdominal pressure is not transmitted, and the heart does not exert any direct mechanical compression on lung parenchyma. As a consequence, the quality of surfactant may be the main determinant of the degree of aeration of the upper lobes and could be more altered in patients with diffuse and patchy attenuations than in patients with lobar attenuations because of differences in the cause of lung injury, as discussed in part 2 [23].

References

1. Bernard GR, Artigas A, Brigham KL, Carlet J, Falke K, Hudson L, Lamy M, Legall JR, Morris A, Spragg R (1994) The American-European Consensus Conference on ARDS. Definitions, mechanisms, relevant outcomes, and clinical trial coordination. Am J Respir Crit Care Med 149: 818–824
2. Murray JF, Matthay MA, Luce JM, Flick MR (1988) An expanded definition of the adult respiratory distress syndrome. Am Rev Respir Dis 138: 720–723
3. Acute Respiratory Distress Syndrome Network (2000) Ventilation with lower tidal volumes as compared with traditional tidal volumes for acute lung injury and the acute respiratory distress syndrome. N Engl J Med 342: 1301–1308
4. Stewart TE, Meade MO, Cook DJ, Granton JT, Hodder RV, Lapinsky SE, Mazer CD, McLean RF, Rogovein TS, Schouten BD, Todd TR, Slutsky AS (1998) Evaluation of a ventilation strategy to prevent barotrauma in patients at high risk for acute respiratory distress syndrome. Pressure- and Volume-Limited Ventilation Strategy Group. N Engl J Med 338: 355–361
5. Dellinger RP, Zimmerman JL, Taylor RW, Straube RC, Hauser DL, Criner GJ, Davis K Jr, Hyers TM, Papadakos P (1998) Effects of inhaled nitric oxide in patients with acute respiratory distress syndrome: results of a randomized phase II trial. Inhaled Nitric Oxide in ARDS Study Group. Crit Care Med 26: 15–23
6. Bigatello LM, Greene RE, Sprung CL, Panacek EA, Straube RC, Zimmerman JL, Maunder RJ, Lanken PN, Pile-Spellmann E, Stanek KS, et al (1994) HA-1 A in septic patients with ARDS: results from the pivotal trial. Intensive Care Med 20: 328–334
7. Anzueto A, Baughman RP, Guntupalli KK, Weg JG, Wiedemann HP, Raventos AA, Lemaire F, Long W, Zaccardelli DS, Pattishall EN (1996) Aerosolized surfactant in adults with sepsis-induced acute respiratory distress syndrome. Exosurf Acute Respiratory Distress Syndrome Sepsis Study Group. N Engl J Med 334: 1417–1421
8. Abraham E, Park YC, Covington P, Conrad SA, Schwartz M (1996) Liposomal prostaglandin E1 in acute respiratory distress syndrome: a placebo-controlled, randomized, double-blind, multicenter clinical trial. Crit Care Med 24: 10–15
9. Gattinoni L, Mascheroni D, Torresin A, Marcolin R, Fumagalli R, Vesconi S, Rossi G, Rossi F, Baglioni S, Bassi F, Nastri F, Pesenti A (1986) Morphological response to positive end expiratory pressure in acute respiratory failure. Computerized tomography study. Intensive Care Med 12: 137–142
10. Gattinoni L, Pesenti A, Torresin A, Baglioni S, Rivolta M, Rossi F, Scarani F, Marcolin R, Cappelletti G (1986) Adult respiratory distress syndrome profiles by computed tomography. J Thorac Imaging 1: 25–30
11. Gattinoni L, Pesenti A, Avalli L, Rossi F, Bombino M (1987) Pressure-volume curve of total respiratory system in acute respiratory failure. Computed tomographic scan study. Am Rev Respir Dis 136: 730–736
12. Gattinoni L, Pesenti A, Bombino M, Baglioni S, Rivolta M, Rossi G, Rossi F, Marcolin R, Mascheroni D, Torresin A (1988) Relationships between lung computer tomographic density, gaz exchange, and PEEP in acute respiratory failure. Anesthesiology 69: 824–832
13. Gattinoni L, Pelosi P, Vitale G, Pesenti A, D'andrea L, Mascheroni D (1991) Body position changes redistribute lung computed tomographic density in patients with acute respiratory failure. Anesthesiology 74: 15–23
14. Gattinoni L, D'andrea L, Pelosi P, Vitale G, Pesenti A, Fumagalli R (1993) Regional effects and mechanism of positive end-expiratory pressure in early adult respiratory distress syndrome. JAMA 269: 2122–2127
15. Gattinoni L, Pelosi P, Crotti S, Valenza F (1995) Effects of positive end-expiratory pressure on regional distribution of tidal volume and recruitment in adult respiratory distress syndrome. Am J Respir Crit Care Med 151: 1807–1814
16. Pelosi P, D'andrea L, Pesenti A, Gattinoni L (1994) Vertical gradient of regional lung inflation in adult respiratory distress syndrome. Am J Respir Crit Care Med 149: 8–13

17. Puybasset L, Rouby JJ, Mourgeon E, Cluzel P, Law-Koune JD, Stewart T, Devilliers C, Lu Q, Roche S, Kalfon P, Vicaut E, Viars P (1995) Factors influencing cardiopulmonary effects of inhaled nitric oxide in acute respiratory failure. Am J Respir Crit Care Med 152: 318–328
18. Umamaheswara Rao GS, Gallart L, Law-koune J-D, Lu Q, Puybasset L, Coriat P, Rouby JJ (1997) Factors influencing the uptake of inhaled nitric oxide in patients on mechanical ventilation. Anesthesiology 87: 823–834
19. Vieira S, Puybasset L, Richecoeur J, Lu Q, Cluzel P, Gusman P, Coriat P, Rouby JJ (1998) A lung computed tomographic assessment of positive end-expiratory pressure-induced lung overdistension. Am J Respir Crit Care Med 158: 1571–1577
20. Puybasset L, Cluzel P, Chao N, Slutsky A, Coriat P, Rouby JJ, CT Scan ARDS Study group (1998) A computed tomography assessment of regional lung volume in acute lung injury. Am J Respir Crit Care Med 158: 1644–1655
21. Vieira S, Puybasset L, Lu Q, Richecoeur J, Cluzel P, Coriat P, Rouby JJ (1999) A scanographic assessment of pulmonary morphology in acute lung injury: signification of the lower inflection point detected on the lung pressure-volume curve. Am J Respir Crit Care Med 159: 1612–1623
22. Puybasset L, Gusman P, Muller JC, Cluzel P, Coriat P, Rouby JJ, and the CT Scan ARDS Study Group (2000) Regional distribution of gas and tissue in acute respiratory distress syndrome. III. Consequences for the effects of positive end-expiratory pressure. Intensive Care Med (in press)
23. Rouby J-J, Puybasset L, Cluzel P, Richecoeur J, Lu Q, Coriat P, CT scan ARDS study group (1999) Regional distribution of gas and tissue in acute respiratory distress syndrome. II. Physiological correlations and definition of an ARDS Severity Score. Intensive Care Med (in press)
24. Austin JHM, Muller NL, Friedman PJ, Hansell DM, Naidich DP, Remy-Jardin M, Webb WR, Zerhouni EA (1996) Glossary of terms for CT of the lungs: recommendations of the Nomenclature Committee of the Fleischner Society. Radiology 200: 327–331
25. Durizch ML, Littleton JT (1994) Chest atlas: radiographically correlated thin section anatomy in five planes. Springer, Heidelberg Berlin New York
26. Mull RT (1984) Mass estimates by computed tomography: physical density from CT numbers. AJR Am J Roentgenol 143: 1101–1104
27. Bland JM, Altman DG (1986) Statistical methods for assessing agreement between two methods of clinical measurement. Lancet I:307–310
28. Hylkema BS, Barkmeijer-Degenhart P, Van der Mark TW, Peset R, Sluiter HJ (1982) Measurement of functional residual capacity during mechanical ventilation for acute respiratory failure. Chest 81: 27–30
29. East TD, Wortelboer PJM, Van Ark E, Bloem FH, Peng L, Pace NL, Crapo RO, Drews D, Clemmer TP (1990) Automated sulfur hexafluoride washout functional residual capacity measurement system for any mode of mechanical ventilation as well as spontaneous respiration. Crit Care Med 18: 84–91
30. Macnaughton PD, Evans TW (1994) Measurement of lung volume and DLCO in acute respiratory failure. Am J Respir Crit Care Med 150: 770–775
31. Wrigge H, Sydow M, Zinserling J, Neumann P, Hinz J, Burchardi H (1998) Determination of functional residual capacity (FRC) by multibreath nitrogen washout in a lung model and in mechanically ventilated patients. Accuracy depends on continuous dynamic compensation for changes of gas sampling delay time. Intensive Care Med 24: 487–493
32. Gevenois PA, Vuyst P, Maertelaer V, Zanen J, Jacobovitz D, Cosio MG, Yernauld JC (1996) Comparison of computed density and microscopic morphometry in pulmonary emphysema. Am J Respir Crit Care Med 154: 187–192
33. Quanjer PH, Tammeling GJ, Cotes JE, Pedersen OF, Peslin R, Yernault JC (1993) Lung volume and forced ventilatory flows. Eur Respir J 6: 5–40
34. Guyton AC (1991) Textbook of medical physiology. Saunders, Philadelphia
35. Falke KJ, Pontoppidan H, Kumar A, Leith DE, Geffin B, Laver MB (1972) Ventilation with end-expiratory pressure in acute lung disease. J Clin Invest 51: 2315–2323
36. Suter PM, Fairley BF, Isenberg MD (1975) Optimum end-expiratory airway pressure in patients with acute pulmonary failure. N Engl J Med 292: 284–289
37. Petty TL, Silvers GW, Paul GWP, Stanford RES (1979) Abnormalities in lung elastic properties and surfactant function in adult respiratory distress syndrome. Chest 75: 571–574
38. Schuster DP, Haller J (1990) Regional pulmonary blood flow during acute pulmonary edema. J Appl Physiol 69: 353–361
39. Staub NC (1974) State of the art: pathogenesis of pulmonary edema. Am Rev Respir Dis 109: 358–372
40. Pelosi P, Crotti S, Brazzi L, Gattinoni L (1996) Computed tomography in adult respiratory distress syndrom: what has it taught us? Eur Respir J 9: 1055–1062
41. Agostini E, D'angelo E, Bonanni MV (1970) Topography of pleural surface pressure above resting volume in relaxed animals. J Appl Physiol 29: 297–306
42. Agostini E, D'angelo E, Bonanni MV (1970) The effect of the abdomen on the vertical gradient of pleural surface pressure. Respir Phys 8: 332–346
43. Tokics L, Strandberg A, Brismar B, et al. (1987) Computerized tomography of the chest and gas exchange measurements during ketamine anaesthesia. Acta Anaesthesiol Scand 31: 684–692
44. Malbouisson LM, Busch CJ, Puybasset L, Lu Q, Cluzel P, Rouby JJ and the CT scan ARDS Study Group (2000) Role of the heart in the loss of aerotion characterizing lower lobes in acute respiratory distress syndrome. Am J Respir Crit Care Med 161: 2005–2012